GELATINE - GLASS MICROBUBBLES HYDROCOLLOID AS POTENTIAL MEDICAL PHANTOM MATERIAL IN COMPUTED TOMOGRAPHY

Ginka Exner[1], Veselina Georgieva[1,2], Yordan Marinov[3], Georgi Tankovski[1], Nikoleta Traikova[2]

[1]*Department of Physics, Faculty of Physics and Technology Plovdiv University "Paisii Hilendarski", Plovdiv 4000 Bulgaria, exner@uni-plovdiv.bg (G.E.); veselina_ngeorgieva@abv.bg (V.G.); georgitankovski@uni-plovdiv.bg (G.T.).*
[2]*UMBAL St. Georgi, 66 Peshtersko Shose Blvd. 4001 Plovdiv, Bulgaria, nikoletatraikova@gmail.com (N.T.).*
[3]*Georgi Nadjakov Institute of Solid State Physics, Bulgarian Academy of Sciences, 72 Tzarigradsko Chaussee Blvd. Sofia 1784, Bulgaria, ymarinov@issp.bas.bg (Y.M.)*

Received 22 August 2025
Accepted 15 September 2025 *DOI: 10.59957/jctm.v61.i1.2026.3*

ABSTRACT

In the present study, gelatine - based hydrocolloids with glass microbubbles were designed and investigated as potential tissue mimicking materials for adipose and lung tissues in Computed tomography. Hydrocolloids contained 0.04 or 0.08 g mL^{-1} gelatine and glass microbubbles in the range 0.04 - 0.28 g.mL^{-1}. Hounsfield units were derived for voltages in the range 70 - 120 kVp. All obtained values were negative with limits from about - 10 HU to about -445 HU. Mechanical performance was also investigated, giving comparatively high Young's modulus up to about 1.2 MPa. Hounsfield units' further decrease might be possible by 3D printing of the hydrocolloids, when printed with a speed from 60 to 90 mL h^{-1}, at a minimum temperature of 40^{o}C. Printability is limited up to 0.20 g mL^{-1} glass microbubbles concentration.

Keywords: medical phantoms, lung and adipose tissues, gelatine hydrocolloids, tissue mimicking materials, computed tomography, glass microbubbles.

INTRODUCTION

Growing concerns on human health issues raises question on appropriate care in the imaging diagnostics. It is especially important for modalities employing ionizing radiation, such as Computed tomography (CT). The professionals are now looking for opportunities to reduce the patient dose, without degrading the quality of the images, and to explore the possibilities for detecting new diseases, or diseases in their early stages, by appropriate adjustment and optimization of the equipment parameters. In carrying out these efforts, medical phantoms are used to replace real patients.

There is a broad spectrum of tested materials for mimic the real biological tissues but the production of phantoms from those materials very often requires special equipment, expensive compounds and it takes long production time [1, 2]. In addition, commercially available phantoms are suited to general purpose cases, such as equipment calibration. Going to personalized medicine, one demands phantoms for each particular case. Therefore they have to be made of cost - effective materials, with easy, eco - friendly and fast production, which can mimic broad spectrum of biological tissues.

Hydrogels meet these recommendations and can be easily shaped by pouring into moulds or filling cavities, matching exactly the desired anatomy [3]. In our previous works we demonstrated, that gelatine hydrogels

with different low budget fillers can be used as tissue mimic materials in CT for broad range of soft tissues such as liver, heart, and muscles [4, 5]. There were difficulties to find appropriate composition to mimic lung tissue and to a certain extent adipose tissue. For such materials, one needs filler with low density. Glass microbubbles (GMB) appear to present a potential for such low density filler, being already used in formulation of tissue mimicking phantoms for ultrasound guided breast biopsy training [6], for B - mode imaging of the blood flow [7] for peripheral nerve blocks, a heart atrium, and a placental phantom for minimally - invasive fetal interventions in ultrasound [8], for diffusion kurtosis imaging for quality assurance in diffusion - weighted magnetic resonance imaging [9], for liver phantom for PET/CT [10], and for transmission X - ray imaging [11], showing a potential in the tissue mimic material formulations.

In the present work, gelatine hydrocolloids with glass microbubbles were fabricated and their potential to mimic adipose and lung tissue in computed tomography was investigate. Their mechanical performance was evaluated by means of Young's modulus and gel strength, in connection with their practical usage.

EXPERIMENTAL

Materials

The main gel matrix consisted of gelatine (bovine, food grade, 250/260 Bloom, CAS 9000 - 70 - 8). Glass microbubbles (3M, Advanced Materials Division, QSM 193.0 Company, USA. K20 type), with a concentration range 0.04 - 0.28 g mL^{-1} were used as filler. Their true density is about 0.20 g cm^{-3}, with and an effective top size of 105 mm. GMB are hollow, so that they form a high air volume fraction in the hydrocolloids, like that of lung tissue. Distilled water (DW) (from MilliQ system) and Glycerol (Gly), (Rai him, Bulgaria, CAS: 56 - 81 - 5) were used as co - solvents in two different DW to Gly ratios 50:50 and 90:10. A disadvantage of water - only hydrogels is their short shelf life of about 2 weeks. Adding Gly increases the durability of the hydrogels to at least 1 year, according to our previous findings.

Gelatine - glass microbubbles hydrocolloids preparation

Two main types of hydrocolloids were prepared: 0.08 g mL^{-1} gelatine concentration with 50 : 50 ratio (Series A), and 0.04 g mL^{-1} gelatine content with 90 :10 ratio (Series B). In both cases, the GMB content range was 0.04 - 0.28 g mL^{-1}. The GMB concentration of 0.28 g mL^{-1} is the upper limit, since above it mixing with the gelatine solution is impossible.

The gelatine powder, measured with an accuracy of 0.1 mg, was mixed with DW and left to swell for 10 mins at room temperature. Then the mixture was transferred onto magnetic stirrer, where it was heated to 63°C, and constantly stirred for 10 mins. GMB and Gly were then added and the final colloidal solution was further stirred for 10 mins at the same conditions.

For CT tests, the hydrocolloid sols were poured into small sterile vessels and tested with the vessels. For mechanical testing, the hydrocolloid sols were poured into home - made holders, so that solid free standing cylindrical samples with diameter and height of 30 mm were prepared. Due to high density differences, GMB and the main sol tend to phase separate (Fig. 1). Therefore, sols were manually stirred until reaching the gelation point to ensure the homogeneity of the samples. The samples were then stored at 4°C for about 24 h prior to the experiments.

Experimental methods

The main requirement for tissue mimicking materials for CT is their X - ray attenuation coefficients to coincide with those of the real biological tissues, in the employed diagnostic photon energy range [12]. Since the study is of a strictly applied nature, CT equipment (Somatom Definition AS64, Siemens, Germany) was used directly to determine the attenuation. We have used parameters, typical for CT tests: tube current of

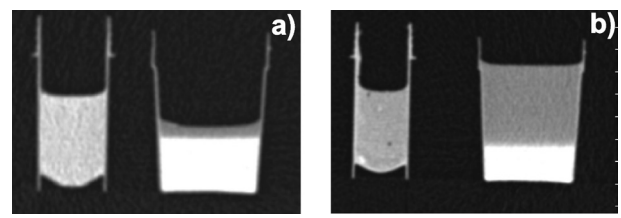

Fig.1. Computed tomography images of Series A samples mechanically agitated (left) and unagitated (right), with a GMB concentration of: (a) 0.04 g mL^{-1} and (b) 0.16 g mL^{-1}. In unagitated samples, grey areas represent the GBM phase, separated from the gelatine sol (white areas).

30 mAs and tube voltages in the range 70 - 120 kVp. Images were taken at a slice thickness 0.6 mm and the acquisition was 64 × 0.6 mm. X - ray attenuation was estimated in terms of Hounsfield units (HU) within regions of interest (ROI) of size 1.5 cm^2 (Eq. (1)):

$$HU = [(\mu - \mu_{H2O})/(\mu_{air} - \mu_{H2O})] \times 1000, \quad (1)$$

where m, μ_{H2O}, and μ_{air} are the linear X - ray attenuation coefficients of the sample, water and air, respectively. DW, placed in the same container as the samples, was also tested. The HU values were derived from the CT images by the help of Singo.Via software, version VB60, with reconstruction kernel medium smooth, B30. The HU values of DW were 4 ± 43 (at 70 kVp) and 3 ± 42 (at 120 kVp). Note that the meaning of the values, given as deviations, represent the inherent voxels colour deviation, due to sample characteristics (water in a plastic container) and the chosen calculation algorithm (kernel). They are not standard deviations in the classical mean. Hence, similar deviations might be expected for the colloids as well.

In the literature, values from -600 HU to -900 HU were reported for lung tissue and from -51 to -215 HU for adipose tissue but the equipment and the experimental conditions are often not specified. Therefore, we performed tests, at the same CT conditions, as those for the hydrocolloids, with fresh porcine tissues (less than 2 h post - mortem), considered to be very close to the human tissues. Our results [4] showed that adipose tissue had -15 ± 36 HU (at 70 kVp) and 23 ± 70 HU (at 120 kVp), whereas for lung tissue the values were -609 ± 66 HU (at 70 kVp) and -611 ± 70 HU (at 120 kVp), when measured in the middle part of the organ, and -551 ± 69 HU (at 70 kVp) and -551 ± 70 HU (at 120 kVp) close to the edge.

Lloyd Universal Instrument LS (Ametek) mechanical tester was used to evaluate the mechanical performance of the hydrocolloids: Young's modulus, as a measure of sample elasticity; and gel strength, giving the mechanical resistance of the sample to compression forces, estimated as the force at maximum compression. Compression tests were performed at room temperature (22°C) in a cyclic loading. A preload of 0.1 N, and a preload speed of 0.1 mm s^{-1} were chosen. Loading was set to 40 % and unloading to 1 %. The cycles were performed at a rate of 0.2 mm s^{-1}.

Scanning electron microscopy (SEM Philips 515) was used to reveal the morphology of the hydrocolloids. Samples for SEM were lyophilized in a chamber TOPT-10B Lab Vacuum Freeze Dryer, Toption Instrument Co. Ltd, China. Prior to the tests, the samples were coated with a thin layer of gold-palladium alloy.

Printability of the colloids was investigated by the help of a syringe infusion pump, with a 20 mL syringe, filled with colloid. The temperature of the colloid was about 40°C. Flow rate varied from 60 to 95 mL h^{-1}. The syringe was connected to a flexible hose, ending with a needle (three different diameters were tested: 0.34 mm - orange, 0.84 mm - green), and 1.36 mm - amber), so that the colloidal jet was injected onto a cold surface (-11°C) for rapid cooling, allowing the sol - gel transition was fast enough to maintain the initial jet size.

RESULTS AND DISCUSSION

In Fig. 2a, HU for Series A are given as a function of the GMB content for 4 different tube voltages. As seen, the HU cover a broad range of values down to -361 HU (at 70 kVp) and -394 HU (at 120 kVp). HU decrease exponentially with GMB concentration. In order to establish the tube voltage dependences, in Fig.2b HU values are given as a function of the voltage. For all GMB concentrations, the dependences are linear. After fitting the data, the intercept and slope dependences are used to derive a master curve of Series A hydrocolloids GMB dependence. The slopes (Fig. 3a) are negative, and their magnitude increases linearly with increasing GMB content: (R^2 = 0.96512):

$$Slope = 0.033\ (\pm 0.002) - 0.024\ (\pm 0.002) \times c_{GMB}, \quad (2)$$

where c_{GMB} is the GMB content in g mL^{-1}, whereas the intercept dependence (Fig. 3b) is exponential (R^2 = 0.99949):

$$Intercept = 502\ (\pm 7)\ exp[-c_{GMB} / 11.9\ (\pm 0.5)] - 367\ (\pm 8) \quad (3)$$

Eq. (2) and Eq. (3) can be used to calculate the needed GMB content to achieve particular HU value. The results show that this series can mimic adipose tissue and some solid nodules or benign and malignant tumours in the lungs (known for their higher density than the healthy lung tissue) but healthy lung tissue HU

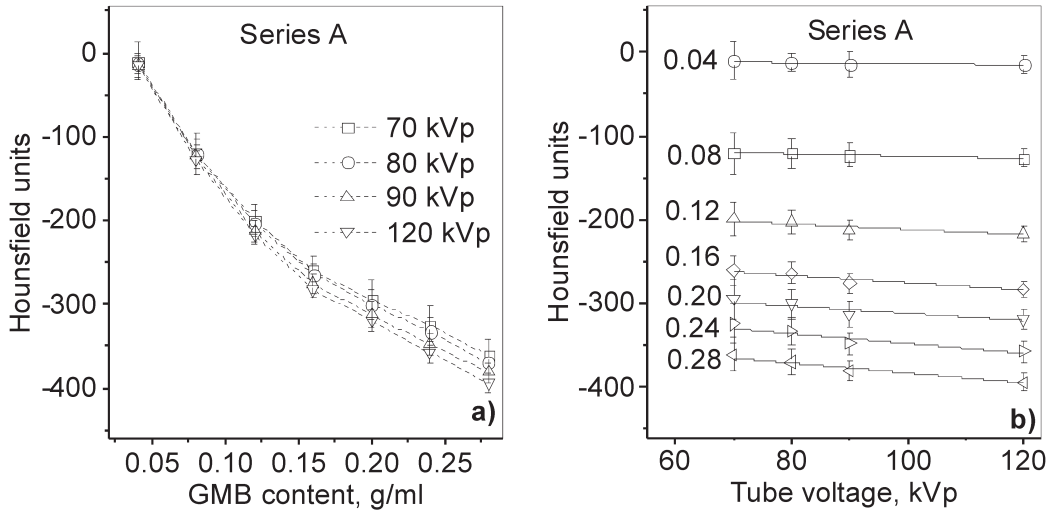

Fig.2. HU dependences for Series A on: (a) GMB content for different tube voltages, given in the figure; (b) the tube voltage, where GMB concentration is given in the figure in g mL^{-1}. The dashed lines in (a) are for eye guidance only, whereas the solid lines in (b) represents linear fits of the data.

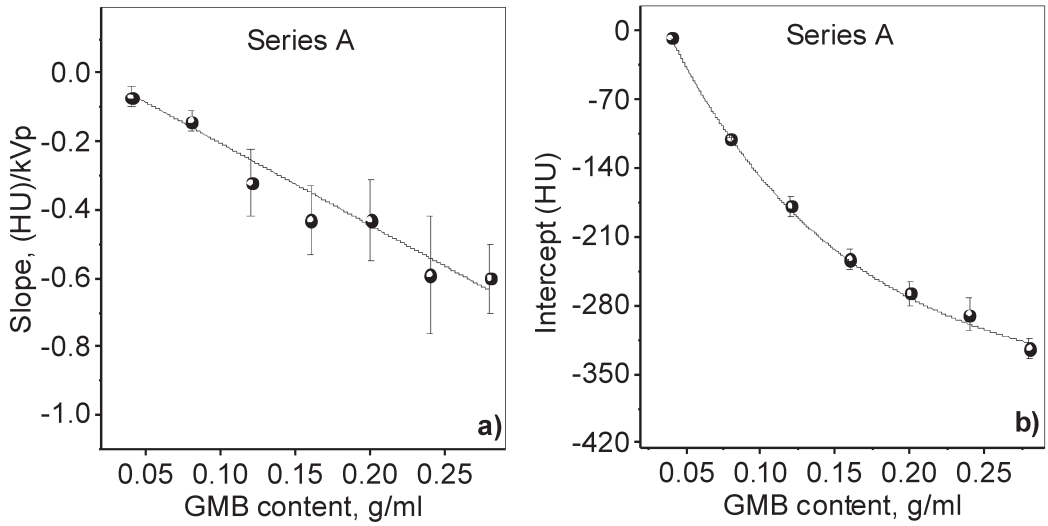

Fig. 3. GMB concentration dependences of Series A of: (a) the slopes; (b) intercepts. The data are taken from linear fits of the data, shown in Fig. 2b. The solid lines represent linear in (a) and exponential in (b) fits. HU stands for Hounsfield units.

were not achieved.

Series A has two main practical advantages: a) comparatively high gelatine content, which ensures mechanical and thermal stability, when stored in refrigeration; b) long shelf - life up to 1 year (at least). Unfortunately, the desired HU values for lung tissue were not reached. Further decrease can be achieved by lowering the gelatine and Gly concentrations. Hence, a new series (Series B) with 0.04 g mL^{-1} gelatine concentration and 90 : 10 DW to Gly ratio was prepared. The results for HU dependences on the GMB content and on tube voltage are presented in Fig. 4.

Similarly to the previous case, master equations for Series B were derived. The slopes (Fig. 5a) are negative and their magnitude increases linearly with increasing GMB content, similar to the previous case ($R^2 = 0.96936$):

$$\text{Slope} = -0.12\ (\pm 0.02) - 0.023\ (\pm 0.002) \times c_{GMB,} \quad (4)$$

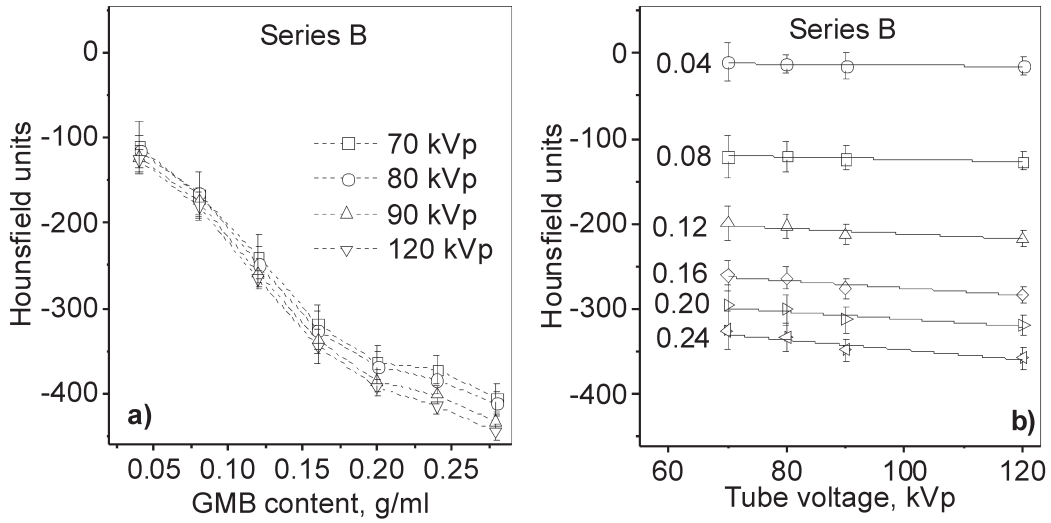

Fig. 4. HU dependences for Series B on: (a) GMB content for different tube voltages, given in the figure; (b) the tube voltage, where GMB concentration is given in the figure in g mL^{-1}. The dashed lines in (a) are for eye guidance only, whereas the solid lines in (b) represents linear fits of the data.

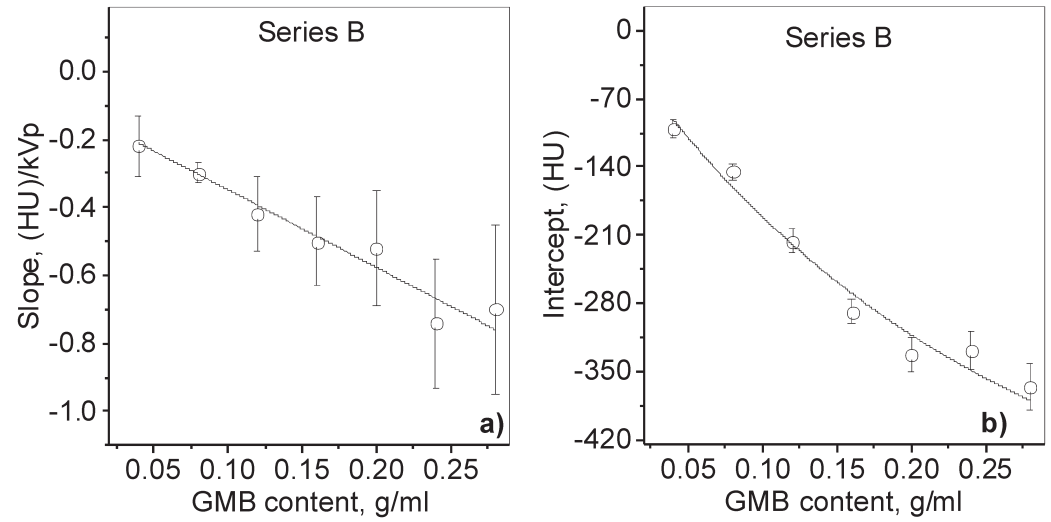

Fig. 5. GMB concentration dependences of Series B (a) the slopes; (b) intercepts. The data are taken from linear fits of the data in Fig. 4b. The solid lines represent linear in (a) and exponential in (b) fits. HU stands for Hounsfield units.

where c_{GMB} is the GMB content in g mL^{-1}, and the intercept dependence (Fig.5b) is exponential again ($R^2 = 0.97492$):

$$\text{Intercept} = 548\ (\pm 81)\ \exp[-c_{GMB} / 25\ (\pm 6)] - 559\ (\pm 94) \quad (5)$$

The slope dependence of Series B is steeper in comparison to that of Series A, and all parameters in Eq. (5) are higher in magnitude with respect to those of Series A, Eq. (3). Series B gives the possibility to reach lower HU values up to -405 HU (at 70 kVp) and -445 HU (at 120 kVp). The conclusion here is that in Series B, indeed the HU are lower but the challenge of obtaining HU of healthy lungs still remains.

Mechanical performance is important from two different reasons: 1) to have sufficient durability during usage and handling; 2) to check the potential of the hydrocolloids to be used as multimodal phantom

materials, for instance in both CT and elastography. The results for both series are shown in Fig.6. Young's modulus and the gel strength increase up to 0.20 g mL^{-1} GMB concentration, showing a good compatibility between the gelatine matrix and the filler. These colloids benefit from the high elastic modulus and hardness of the GMB. At higher concentrations both parameters deteriorate, suggesting changes in the colloid microstructure. Nevertheless, all colloids remained intact after the tests and their mechanical performance is suitable for mechanical manipulation during daily usage. The values of Young's modulus vary from 0.05 to 1.2 MPa, being much higher than those of adipose (0.001 - 0.30 MPa) and lung (0.001 - 0.16 MPa) tissues, excluding potential multimodal (CT and elastography) applications of these colloids. Even though some authors used successfully similar hydrocolloids of gelatine, GMB and some more additives, as tissue mimicking materials for photoacoustic imaging of soft tissues, where matching of ultrasound velocity and attenuation were achieved, together with appropriate optical properties [13].

To gain deeper understanding on the processes, leading to the decreasing values of the mechanical parameters, the hydrocolloid morphology was revealed by SEM. Representative SEM images at varying co - solution concentration for 0.08 g mL^{-1} GMB content are shown in Fig.7. The hydrocolloids with DW only, 100:0 ratio (Fig. 7a) are highly porous. GMB are interlocked in the gelatine network, partially covered with gelatine. The network is denser (smaller pore sizes) in comparison to Series B (Fig. 7c). Gly has plasticizing effect, so that the gelatine - Gly - DW mixture forms shells around the individual GMB (Fig. 7b). At lower gelatine concentration porosity remains high and the shells have granular - like structure (Fig. 7d). Increasing gelatine content, in the presence of Gly, improves the structure in the sense that the shells are thicker and they look smoother. Based on the results here, the decrease in Young's modulus and gel strength at large GMB contents seems to be a consequence of the inability to form a stable gel due to the spatial limitation of contact between individual gelatine molecules as their volume fraction decreases.

Our observations so far showed that further reduction of HU by varying gelatine, Gly, and GMB is hardly achievable. Another option, already used in practice for obtaining phantom materials in medicine, is 3D printing [14 - 17]. The initial conducted experiments, even requiring 3D process optimisations, showed good printability of all colloids with GMB content up to 0.20 g mL^{-1}. At higher contents, the sol was too dense to form jet. The colloids clogged the needle with the smallest diameter 0.34 mm but the jets flow smoothly and were constant in shape for the other needles (0.84 mm and 1.36 mm diameters). Representative photographs of the printed free - hand filaments are given in Fig.8.

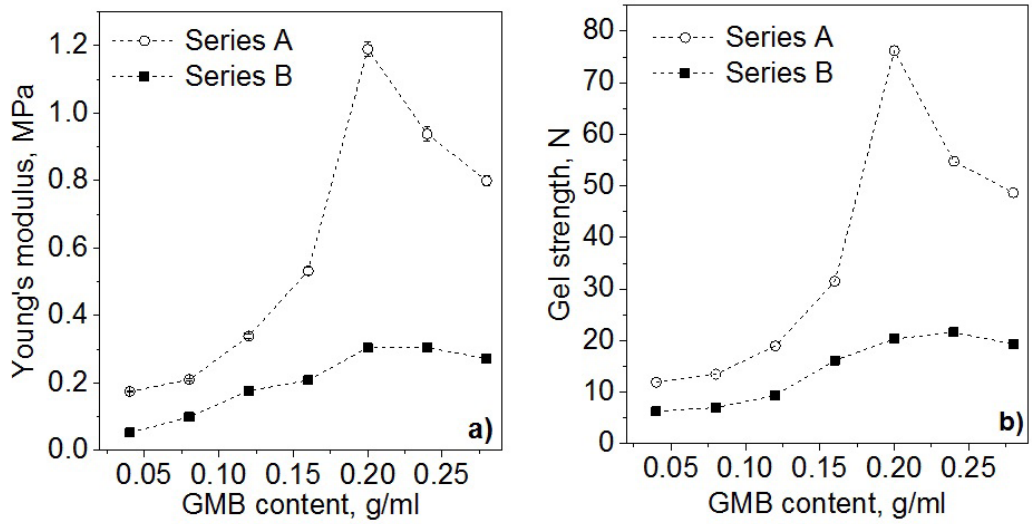

Fig. 6. GMB concentration dependences for both series of: (a) Young's modulus; (b) gel strength. The dashed lines are eye guidance only.

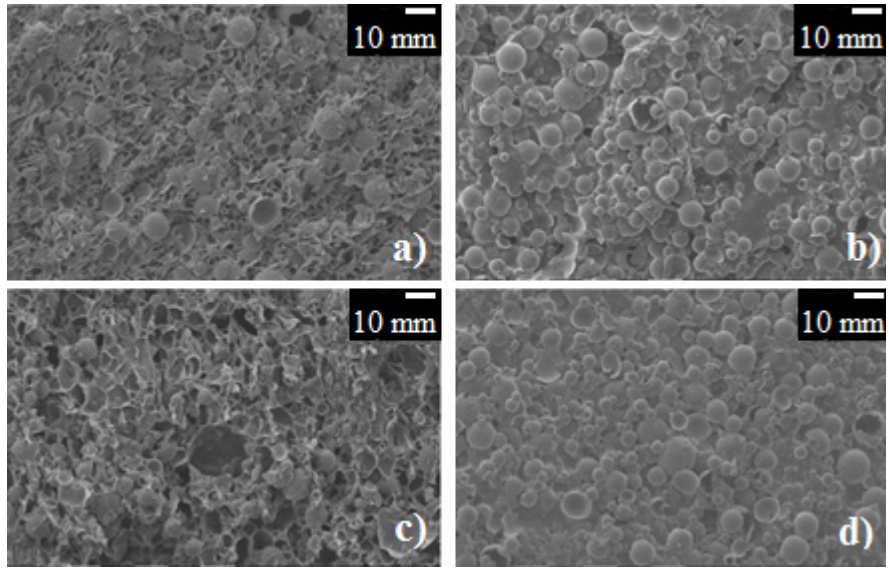

Fig. 7. Representative SEM images of some hydrocolloids, taken at 80 kV: (a) Series A, 0.08 g mL^{-1} GMB, 100 : 0 DW to Gly ratio; (b) Series A, 0.08 g mL^{-1} GMB, 70 : 30 ratio;(c) Series B, 0.08 g mL^{-1} GMB, 100 : 0 ratio; (d) Series B, 08 g mL^{-1} GMB, 70 : 30 ratio.

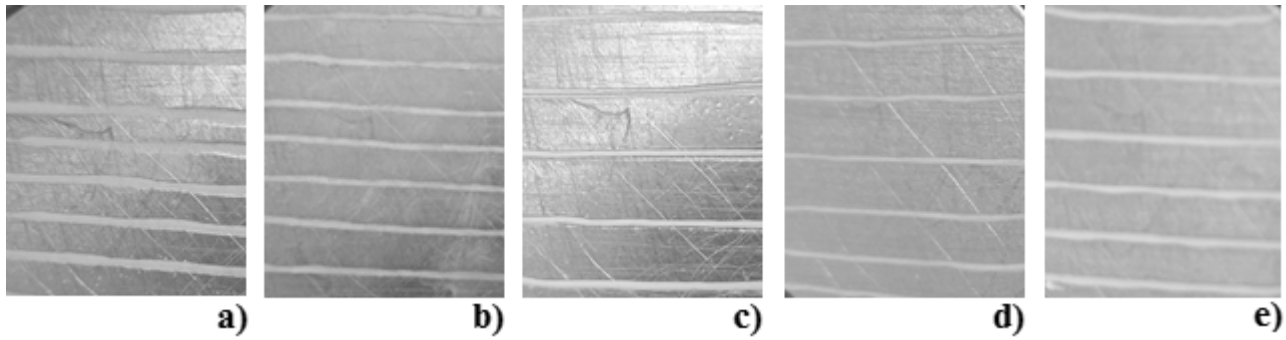

Fig. 8. Photographs of printed filaments from the investigated hydrocolloids of Series A: (a) 0.04 g mL^{-1} GMB, speed of 90 mL h^{-1}; (b) 0.04 g mL^{-1} GMB, speed of 95 mL h^{-1}; (c) 0.08 g mL^{-1} GMB, speed of 50 mL h^{-1}; (d) 0.08 g mL^{-1} GMB, speed of 85 mL h^{-1}; (e) 0.08 g mL^{-1} GMB, speed of 90 mL h^{-1}.

CONCLUSIONS

Hydrocolloids consisting of gelatine, distilled water and glycerol as co - solvents, and glass microbubble, as high air fraction filler, were prepared and their potential as tissue mimicking materials for adipose and lung tissue in Computed tomography was investigated. Hounsfield units of the hydrocolloids span between -10 HU (at 70 kVp, Series A) to -445 HU (at 120 kVp, Series B), fully covering Hounsfield units of adipose tissue and corresponding to some hard nodules and benign or malignant tumours in lung tissue but the challenge remains to mimic healthy lungs. One possible way of further HU lowering would be a 3D printing of porous structures. We conducted preliminary studies, which showed good printability of the hydrocolloids up to 0.20 g mL^{-1} GMB concentration, at speeds of 60 - 95 mL h^{-1}, with a needle (nozzle) diameter of at least 0.84 mm.

Acknowledgments

This work was supported by the Ministry of Education and Science of Bulgaria (MESB), through the National Research Fund of Bulgaria (research project "Liquid crystal nanocomposites for applications in photonics, sensors and biomedicine", No. KP-06-N58/6/2021).

Authors' contributions

G.E. conceived the idea of the study, designed the hydrocolloids, planned the experiments, performed data treatment, write the manuscript. V.G. and G.T. formulated the hydrocolloids, performed the CT and mechanical testing experiments, and deals with the data treatment. Y. M. supervised the project, performed SEM experiments. N.T. supported the CT measurements. All authors provided critical feedback and helped shape the research, analysis and manuscript.

REFERENCES

1. C.K. McGarry, L.J. Grattan, A.M. Ivory, F. Leek, G.P. Liney, Y. Liu, P. Miloro, R. Rai, A.P. Robinson, A.J. Shih, B. Zeqiri, C.H. Clark, Tissue mimicking materials for imaging and therapy phantoms: a review, Phys. Med. Biol., 65, 2020, 23TR01. doi: 10.1088/1361-6560/abbd17
2. V. Filippou, C. Tsoumpas, , Recent advances on the development of phantoms using 3D printing for imaging with CT, MRI, PET, SPECT, and Ultrasound, Med. Phys., 45, 9, 2018, e740 e760. doi: 10.1002/mp.13058
3. E. Lennie, C. Tsoumpas, S. Sourbron, Multimodal phantoms for clinical PET/MRI, EJNMMI Physics, 8, 2021, 62. doi: 10.1186/s40658-021-00408-0
4. V. Georgieva, G. Tankovski, N. Traikova, G. Exner, Effects of different fillers on hydrogels for application as tissue-substitute materials for computed tomography phantoms, J. Phys. Conf. Ser., 2952, 2025, 012014. doi:10.1088/1742-6596/2952/1/012014
5. G. Tankovski, V. Georgieva, N. Traikova, G. Exner, Engineering the mechanical and X-ray attenuation properties of gelatine composite hydrogels with a potential for tissue mimicking materials, J. Phys. Conf. Ser. 2952, 2025, 012015. doi: 10.1088/1742-6596/2952/1/012015
6. S.L. Vieira, T.Z. Pavan, J.E. Junior, A.A. Carneiro, Paraffin-gel tissue-mimicking material for ultrasound-guided needle biopsy phantom, Ultrasound Med. Biol., 39, 2013, 2477-2484. doi: 10.1016/j.ultrasmedbio.2013.06.008
7. K. Funamoto, O. Yamashita, T. Hayase, Poly(vinyl alcohol) gel ultrasound phantom with durability and visibility of internal flow. J. Med. Ultrason., 42, 2015, 17-23. doi: 10.1007/s10396-014-0560-x
8. E. Maneas, W. Xia, D.I. Nikitichev, B. Daher, M. Manimaran, R.Y.J. Wong, C.-W. Chang, B. Rahmani, C. Capelli, S. Schievano, G. Burriesci, S. Ourselin, A.L. David, M.C. Finlay, S.J. West, T. Vercauteren, A.E. Desjardins, Anatomically realistic ultrasound phantoms using gel wax with 3D printed moulds, Phys. Med. Biol., 63, 2018, 015033. doi: 10.1088/1361-6560/aa9e2c
9. Z.G. Portakal, S. Shermer, C. Jenkins, E. Spezi, T. Perrett, N. Tuncel, J. Phillips, Design and Characterization of tissue-mimicking gel phantoms for diffusion kurtosis imaging, Med. Phys., 45, 6, 2018, 2476-2485. doi:10.1002/mp.12907
10. Y.H. Kao, O.S. Luddington, S.R. Culleton, R.J. Francis, J.A. Boucek, A Gelatin liver phantom of suspended 90Y resin microspheres to simulate the physiologic microsphere biodistribution of a postradioembolization liver, J. Nucl. Med. Techn., 42, 4, 2014, 265-268. doi:10.2967/jnmt.114.145292
11. E. Dahal, A. Badal, A. Zidan, A. Alayoubi, T. Hagio, S. Glick, A. Badano, B. Ghammraoui, Stable gelatin-based phantom materials with tunable x-ray attenuation properties and 3D printability for x-ray imaging, Phys. Med. Biol., 63, 9, 2018, 09NT01. doi:10.1088/1361-6560/aabd1f
12. P. Homolka, A. Gahleitner, M. Prokop, R. Nowotny, Phys. Med. Biol., 47, 2002, 2907-2916
13. E. Amidi, G. Yang, K.M.S. Uddin, R. Wahidi, Q. Zhu, Low-cost ultrasound and optical gelatin-based phantoms, Proc. SPIE, 10878, 2019, 108784A. doi: 10.1117/12.2507938
14. K. Bliznakova, N. Dukov, Z. Bliznakov, V. Petkova, V. Nastev, V. Eleftheriadis, P. Papadimitroulas, N. Okkalidis, E, Ivanova, T. Teneva, G. Todorov, G. Mettivier, P. Russo, Assessment of physical phantoms produced in the PHENOMENO project utilizing three fused filament fabrication approaches, Physica Medica, 136, 2025, 105061. doi:10.1016/j.ejmp.2025.105061
15. E. Colvill, M. Krieger, P. Bosshard, P. Steinacher, B.A.R. Schnidrig, T. Parkel, I. Stergiou, Y. Zhang, M. Peroni, S. Safai, D.C. Weber, A. Lomax, G. Fatto, Anthropomorphic phantom for deformable lung and liver CT and MR imaging for radiotherapy, Phys. Med. Biol., 65, 2020, 07NT02. doi: 10.1088/1361-6560/ab7508

16. K. Mei, M. Geagan, L. Roshkovan, H.I. Litt, G.J. Gang, N. Shapira, J.W. Stayman, P.B. Noël, Three-dimensional printing of patient-specific lung phantoms for CT imaging: Emulating lung tissue with accurate attenuation profiles and textures, Med. Phys. 49, 2, 2022, 825-835. doi:10.1002/mp.15407
17. J. Lai, C. Wang, M. Wang, 3D printing in biomedical engineering: Processes, materials, and applications, Appl. Phys. Rev., 8, 2, 2021, 021322. doi: 10.1063/5.0024177